Optics Letters

Coherent propulsion with negative-mass fields in a photonic lattice

Yumiao Pei,[1] Yi Hu,[1,*] Ping Zhang,[1] Chunmei Zhang,[1] Cibo Lou,[2] Christian E. Rüter,[3] Detlef Kip,[3] Demetrios Christodoulides,[4] Zhigang Chen,[1,5,6] and Jingjun Xu[1,7]

[1]The MOE Key Laboratory of Weak-Light Nonlinear Photonics, TEDA Applied Physics Institute and School of Physics, Nankai University, Tianjin 300457, China
[2]Faculty of Science, Ningbo University, Ningbo 315211, China
[3]Faculty of Electrical Engineering, Helmut Schmidt University, 22043 Hamburg, Germany
[4]CREOL/College of Optics, University of Central Florida, Orlando, Florida 32816, USA
[5]Department of Physics and Astronomy, San Francisco State University, San Francisco, California 94132, USA
[6]e-mail: zgchen@nankai.edu.cn
[7]e-mail: jjxu@nankai.edu.cn
*Corresponding author: yihu@nankai.edu.cn

Received 14 June 2019; revised 25 October 2019; accepted 29 October 2019; posted 31 October 2019 (Doc. ID 370069); published 5 December 2019

In this Letter, we demonstrate the first, to the best of our knowledge, *coherent* propulsion with negative-mass fields in an optical analog. We observe a self-accelerating state, driven by a nonlinear coherent interaction of its two components that are experiencing diffractions of opposite signs in a photonic lattice, which is analogous to the interaction of two objects with opposite mass signs. Surprisingly, the coherent propulsion is highly immune to the initial phase of the two components, which is in sharp contrast with the behavior encountered in traditional coherent wave interactions. Compared to its *incoherent* counter-part, the coherent propulsion exhibits an enhanced acceleration.

https://doi.org/10.1364/OL.44.005949

In the framework of classical mechanics [1,2], positive-mass matter is illustrated as continuously driven by hypothetical negative-mass matter, merely by their mutual interaction. The action–reaction symmetry, governed by Newton's third law, is broken in such a captivating negative-mass propulsion, yet, counterintuitively, abiding to both energy and momentum conservation. To the best of our knowledge, such a propulsion has been first demonstrated by using two optical pulses experiencing dispersions of opposite signs [3,4], analogous to two objects with opposite mass signs. Quite recently, it has also been realized in a mass–spring system [5] and in a photonic lattice, where self-bending light was observed [6]. However, limited by classical mechanics, where the concept of negative-mass propulsion stems from, those prior studies overlooked the coherence effects that may strengthen the interaction force as simply inferred from a constructive interference.

Indeed, coherence and interference were even rarely involved in the interplay of two entities of the same mass until the advent of solitons [7] that exhibit properties of both waves and particles, and hence become excellent tools to uncover the mechanism behind coherent interactions. As mostly demonstrated in nonlinear optics [8–12] and Bose–Einstein condensates [13,14], the phase difference between solitons enables fruitful interaction scenarios. For instance, in homogenous media, two bright solitons initially set to be in phase or out of phase exhibit attraction or repulsion [9]. Those dramatically distinct interaction behaviors were also realized in the coherent interaction of lattice solitons in photonic lattices [11,12]. Although coherence brings about an ease control of the interacting force between solitons, it is detrimental for maintaining a unidirectional propulsion against environmental perturbations. However, as we shall demonstrate here, this scenario is changed dramatically for a negative-mass propulsion in the coherent regime, where coherent interaction leads to an altogether high stability.

In this Letter, we demonstrate the first coherent propulsion with negative-mass fields in an optical analog. A coherent self-accelerating state is realized in a photonic lattice, driven by the interaction of its intrinsic components of positive-mass and negative-mass fields. In sharp contrast with the behavior encountered in traditional coherent wave interactions, the coherent propulsion shows a high immunity to the initial phase variation of the two fields. In addition, it exhibits an enhancement of acceleration as compared with its incoherent counterpart.

Our experimental setup is schematically illustrated in Fig. 1(a). A collimated broad beam (via expanding a CW green laser light at the 532 nm wavelength) illuminates a spatial light modulator (SLM, PLUTO, Holoeye) imposed with a proper phase pattern. Then through a $4f$ system (a couple of cylindrical lenses) together with a $10\times$ microscope objective, we generate the desired input beam at the front facet of a waveguide array (the length is 14 mm and the lattice period Λ is 6.8 μm), which is fabricated by titanium in-diffusion in a nonlinear

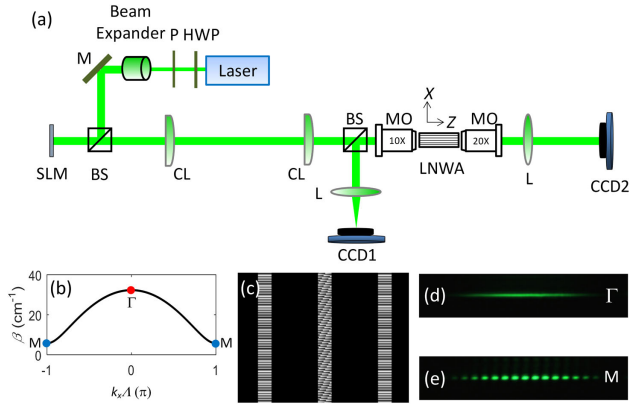

Fig. 1. (a) Experimental setup. P, polarizer; HWP, half-wave plate; M, mirror; CL, cylindrical lens with $f = 200$ mm; L, convex lens with $f = 150$ mm; BS, 50/50 beam splitter; MO, microscope objective; LNWA, lithium niobate waveguide array; CCD1, CCD2, charged coupled device. (b) Dispersion diagram of the first Bloch band associated with the lattice being tested. (c) Phase pattern employed for generating the Γ- and M-beam simultaneously. (d) and (e) Experimentally captured input beams to match the modes of the band edges in (b).

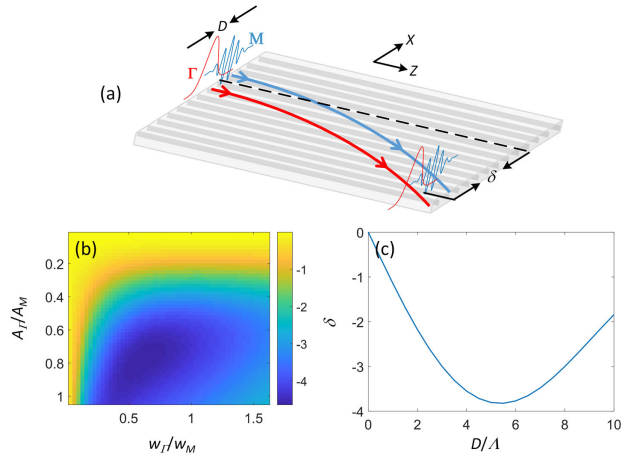

Fig. 2. (a) Schematic coherent propulsion. (b) and (c) Numerically calculated beam center shifts δ of the combined beam at the output for different input conditions: (b) $A_M = 0.96$ and $W_M = 6.2$; (c) $A_M = 2A_\Gamma = 0.96$, $W_M = W_\Gamma = 6.2$. Each pixel in (b) corresponds to the maximum absolute value of δ when scanning the spacing between the Γ- and M-beam.

photorefractive $LiNbO_3$ crystal that has a self-defocusing nonlinearity arising from the bulk photovoltaic effect [6]. As a result of the periodic refractive index distribution, the diffraction relationship in this optical structure can be described by the Bloch bands [15]. Figure 1(b) presents the first band (propagation constant β versus transverse vector k_x) of our sample in the first Brillouin zone (BZ). Analog to the effective mass defined for electronic states in crystals [16], the optical beams that can match the Bloch modes around the top (Γ) and the bottom (M) edges would undergo normal and anomalous diffraction, and thus they are defined as positive- and negative-mass fields (denoted as Γ-beam and M-beam), respectively. Considering that the two fields are generally produced by a Gaussian beam and a cosine-Gaussian beam, the phase mask shown in Fig. 1(c) is employed to impose on the SLM. It has three stripes with the same linear phase modulation (wrapped between 0 and 2π) along the vertical direction, allowing parts of the beam that do not illuminate on the stripes to be filtered, and leaving only three narrow beams to inject into the 10× objective. Apart from the vertical modulation, its central stripe is overlapped with a linear phase modulation along the horizontal direction to control the spacing (denoted as D) between the Γ- and M-beam at the input. Individual Γ- and M-beams can be generated by switching on the phase patterns that merely duplicate the central and outer stripes in Fig. 1(c), respectively. Their profiles, featured with an in-phase and a stagger-phase structure, are shown as typical examples in Figs. 1(d) and 1(e), as captured by CCD1.

Mathematically, the fields of the Γ- and M-beams can be expressed as $\psi_\Gamma = A_\Gamma \exp[(x - D/\Lambda)^2/W_\Gamma^2]\exp(i\Delta\phi)$ and $\psi_M = A_M \cos(\pi x)\exp(x^2/W_M^2)$, where x is the transverse dimension normalized by the lattice constant, A_Γ and A_M are the amplitudes, W_Γ and W_M determine the beam widths, and $\Delta\phi$ is the phase difference between the two beams, which can be readily controlled by the phase mask. Without loss of generality, D is kept positive. As presented in Ref. [6], the Γ- and M-beams show inverted behaviors when encountering a negative index change embedded in a uniform lattice. The former tends to be repelled, while the latter tends to be attracted. Under the action of the self-defocusing nonlinearity, both the Γ- and M-beams induce negative refractive index changes. When the two beams propagate together with a beam-center mismatch, they can shift to the same direction due to the symmetry breaking of action–reaction, which is the origin of synchronized self-acceleration or propulsion, as schematically shown in Fig. 2(a). Parameters of both beams should be carefully chosen for a better observation of the propulsion in our short crystal with a saturable nonlinearity. One should, first of all, choose a proper beam width and peak intensity for the M-beam, since the spreading for one side of the beam needs to be suppressed by the nonlinear effect [3]. According to our experimental conditions, $A_M = 0.96$ and $W_M = 6.2$ for the M-beam are employed, which can lead to a soliton-like propagation in the absence of the Γ-beam.

Then, we use numerical simulations to choose the parameters of the Γ-beam. Since the nonlinear evolution is mainly driven by the photovoltaic-photorefractive effect rather than the thermal effect, the steady state of the beam propagation can be simulated using the following nonlinear Schrödinger equation in a normalized form [17]:

$$i\frac{\partial\psi}{\partial z} + \frac{\partial^2\psi}{\partial x^2} + V(x)\psi = \gamma\frac{|\psi|^2}{1+|\psi|^2}\psi, \tag{1}$$

where ψ is the slowly varying complex amplitude of a beam; x and z are the dimensionless transverse and longitudinal coordinates, normalizing the laboratory coordinates X, Z by Λ and $2k\Lambda^2$ (k is the wavenumber in the crystal), respectively; $V(x) = 2k\Lambda^2 k_0 A\cos^2(\pi x)$ is the normalized periodic index change of the waveguide array with A being the lattice modulation depth and k_0 being the wavenumber in vacuum; and $\gamma = k_0^2 n^4 \Lambda^2 \gamma_{33} E_{pv}$ is the normalized nonlinear coefficient with n being the unperturbed refractive index of the crystal, γ_{33} being the electro-optic coefficient, and E_{pv} being the photovoltaic field. In simulations (performed by the split-step beam propagation method), the experimental parameters, i.e., $n = 2.3$, $\gamma_{33} = 280$ pm/V, $E_{pv} = 400$ V/cm, and

$A = 5.0 \times 10^{-4}$ are adopted. By using different parameters of the Γ-beam, we record the beam center shift at the output that is defined as $\delta = C_{\mathrm{NL}} - C_L$, where C_{NL} and C_L are the beam centers of a nonlinear and the corresponding linear (i.e., by letting $\gamma = 0$) output, and both of them can be calculated by $\int x|\psi|^2 \mathrm{d}x / \int |\psi|^2 \mathrm{d}x$. Since the spacing D is positive, a negative value of δ is expected [6]. A larger absolute value of δ indicates a stronger acceleration of the propulsion. One can see from Fig. 2(b) that there is an optimized parameter condition for the Γ-beam to reach the maximum shift of the beam center, i.e., $A_\Gamma / A_{\mathrm{M}} \approx 0.8$, $W_\Gamma / W_{\mathrm{M}} \approx 0.6$. We intend to choose a condition close to this optimized one, while considering simplifying the experimental design. In the end, the central stripe in the phase pattern imposed on SLM is set to have the same width with the outer ones [Fig. 1(c)], corresponding to the Γ-beam having the same beam width as the M-beam, but with a half-peak intensity. In this case, although the shift of the beam center is near one lattice constant less than the ideal case, it is still considerable for experimental observation. Under the input condition we employed, there is an optimized spacing (about six times of the lattice constant) between the Γ- and M-beam for realizing the largest shift of the beam center, as seen from Fig. 2(c). Using this spacing, one can realize an enhanced acceleration by simply increasing the input power of the two beams together, but it is not recommended to use a quite large input power considering the saturable nonlinearity that may reduce the nonlinear propulsion.

In the first experiment, the two mutually coherent beams are launched simultaneously into the waveguide array with an equal phase (i.e., $\Delta\phi = 0$) and a total input power of 9.83 μW. Their spacing is set to be the optimized value, i.e., about six times of the lattice constant. Taking the advantage of the noninstantaneous photorefractive response, we are able to record the temporal evolution of the beams existing in the lattice. As summarized in Fig. 3(a), the combined output evolves from a widely spread distribution to a somewhat localized pattern; meanwhile the overall beam center (defined as $\int X\mathrm{d}X \int I\mathrm{d}Y / \iint I\mathrm{d}X\mathrm{d}Y$, where I is the light intensity) at the steady-state moves along the $-X$ direction. The localization is attributed to discrete self-trapping [17–20], while the lateral movement of the whole beam takes place when its two components with opposite diffraction signs break the action–reaction symmetry during interaction [6]. For comparison, the output for the two beams having zero spacing (overlapped centers at input) is presented in Fig. 3(b), where the lateral shift of the beam center is almost not noticed. Numerical beam propagations simulated by using Eq. (1) at a distance longer than the sample length are shown in Figs. 3(c) and 3(d). The combined beam experiences a self-accelerating effect for the case of non-zero spacing between the Γ- and M-beam [Fig. 3(c)], while its pattern always remains symmetrical about $X = 0$ for the other case [Fig. 3(d)]. Employing other initial phase differences, the evolutions of coherent propulsion look quite similar (this feature will be revisited later). The momentum change of the light is accordingly revealed in the (spatial) spectrum domain [Figs. 3(e, f)]. In the coherent propulsion, both positive- and negative-mass components, located at the center ($k_x\Lambda = 0$) and boundary ($k_x\Lambda = \pm\pi$) of the 1st BZ, respectively, exhibit a net shift due to the self-accelerating effect.

Next, we study the influence of the initial phase difference between the Γ- and M-beam on the coherent propulsion. The phase difference can be altered at ease by adding a constant

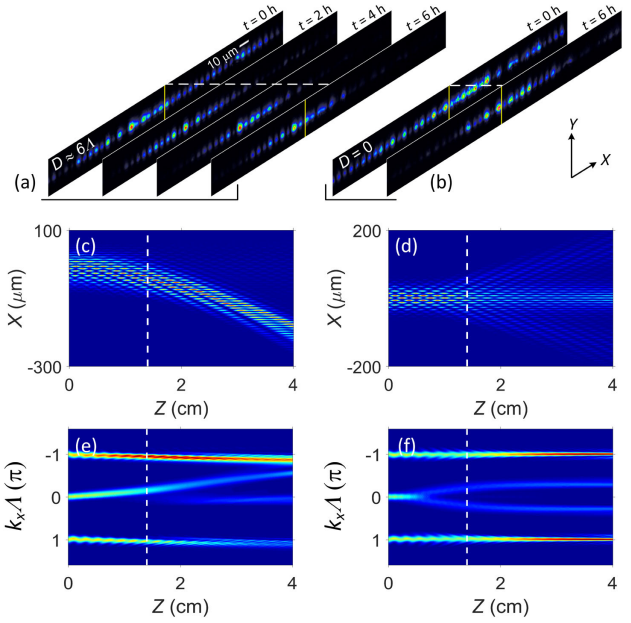

Fig. 3. (a) and (b) Temporal evolution of the beam output under the action of the nonlinearity when the initial spacing (D) between the Γ- and M-beam is (a) about six times of the lattice constant Λ and (b) zero, where the yellow lines mark the "center of mass." Notice that the outputs in (a) and (b) are shown at different intensity scales. (c) and (d) show the numerical simulations of the beam propagations in a steady state corresponding to (a) and (b), respectively, and the dashed white lines mark the output location of our sample. (e) and (f) Spatial spectral evolution corresponding to (c) and (d), respectively.

value to the central stripe in Fig. 1(c). In the experiment, three different input conditions (i.e., $\Delta\phi = 0$, $\pi/2$, and π) are considered, and a larger input power (20.52 μW) is injected aiming for an evident distinction from the incoherent case that will be studied later. The nonlinear outputs, recorded at a steady state, are shown in Figs. 4(a)–4(c). Although the output profiles (calculated by $\int I\mathrm{d}Y$) look inequivalent, the overall beam center (as calculated from experimental data) changes hardly for the three different cases. This phenomenon holds unchanged even for a much longer propagation distance in simulations. The phase-insensitive behavior for beam interactions arises from the beating effect along the waveguide array. For our example, the propagation constant difference at Γ- and M-points [Fig. 1(b)] is estimated to be $\sim 26\ \mathrm{cm}^{-1}$, corresponding to a short beating length of 0.039 cm. Consequently, for a sufficiently long distance, the coherent propulsion becomes immune to the initial phase fluctuation. To verify our expectation, we simulate the beam propagation up to the sample length by employing phase differences varying from 0 to 2π, and we calculate the relative change of the central position defined by $\Delta\delta = (\delta - \bar{\delta})/\bar{\delta} \times 100\%$, where $\bar{\delta} = \int_0^{2\pi} \delta \mathrm{d}\phi/(2\pi)$ is the beam center's average shift that varies along the propagation. The numerical calculations are summarized in Fig. 4(e). At the very early stage of the propagation, the beam center of the combined beam varies dramatically with the initial phase difference. After a short distance (say, $Z = 0.25$ cm), the relative change of the beam's central position becomes small and tends to be smaller along the propagation. This indicates that the coherent

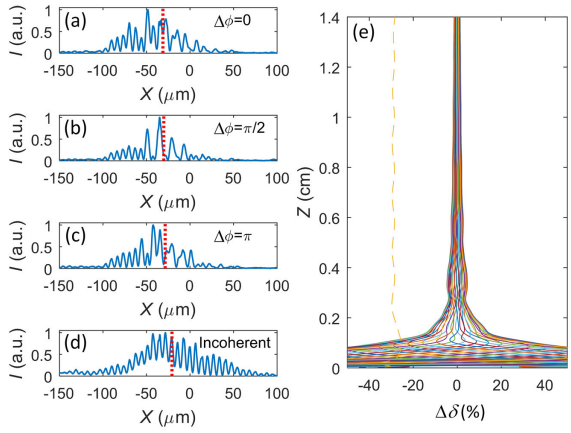

Fig. 4. (a)–(d) Measured nonlinear output intensity profiles (a)–(c) for the coherent case with three typical initial phase differences between the Γ- and M-beam, and (d) for the incoherent case. (e) Numerically calculated change of the beam center position relative to the average change in a coherent propulsion using various initial phase conditions (here we employ 65 phase differences equally distributed between 0 and 2π), where the dashed line corresponds to the incoherent case for reference.

propulsion can resist the initial phase variation, as observed in our experiment [Figs. 4(a)–4(c)].

Then we switch the interaction to the incoherent regime. For this purpose, we make a movie including 60 phase patterns similar to Fig. 1(c) to change the phase difference (i.e., $\Delta\phi$) gradually from 0 to 2π. This movie is played in a loop mode at the maximum refresh rate (i.e., 60 Hz) of the SLM. Since the fluctuation of phase difference between the Γ- and M-beam is much faster than the nonlinear response of our crystal [21], the interaction of the two beams becomes incoherent. Thus, except for the phase relationship between the Γ- and M-beam, the experiments for coherent and incoherent propulsion are performed under the same conditions. After the same evolution period as for the coherent case, the nonlinear outputs for the Γ- and M-beams are recorded. Their intensity overlapping is shown in Fig. 4(d). Compared with the coherent cases, the output profile now shows a smaller shift of the beam's central position around 21 μm, which is 30% less than the averaged lateral shift (∼ 30 μm) for the three coherent cases. In simulation, the incoherent interaction is calculated using the following coupled equations:

$$i\frac{\partial\psi_\Gamma}{\partial z}+\frac{\partial^2\psi_\Gamma}{\partial x^2}+V(x)\,\psi_\Gamma=\gamma\frac{|\psi_\Gamma|^2+|\psi_M|^2}{1+|\psi_\Gamma|^2+|\psi_M|^2}\psi_\Gamma,$$

$$i\frac{\partial\psi_M}{\partial z}+\frac{\partial^2\psi_M}{\partial x^2}+V(x)\,\psi_M=\gamma\frac{|\psi_\Gamma|^2+|\psi_M|^2}{1+|\psi_\Gamma|^2+|\psi_M|^2}\psi_M. \quad (2)$$

The numerical calculation (∼ 28.4%) on the deduction of the beam center shift is close to the measurement (i.e., 30%), which in turn shows that the coherent propulsion exhibits nearly a 40% enhancement of the acceleration that is roughly assumed as a constant. This is attributed to a stronger nonlinearity that appears in the coherent case due to constructive interference. In essence, larger refractive index changes can be induced, leading to more intense beam deflections compared to the incoherent propulsion.

In conclusion, in this Letter, we have demonstrated the first coherent propulsion with analog positive- and negative-mass fields in a simple optical setting, renewing the picture of negative-mass propulsion proposed decades ago. Using a photonic platform, we have shown a stable and synchronized self-accelerating state of two mutually coherent fields of opposite mass signs, immune to their initial phase difference. Compared with its incoherent counterpart, the coherent propulsion exhibits altogether an enhanced acceleration. Our work may bring about new possibilities for fundamental studies involving negative mass in a variety of physical systems as well as for sought-after applications based on the principles of negative-mass propulsion.

Funding. The National Key R&D Program of China (2017YFA0303800); National Natural Science Foundation of China (11504186, 61575098, 91750204); 111 Project in China (B07013); Natural Science Foundation of Ningbo (ZX2015000617).

REFERENCES

1. R. L. Forward, J. Propul. Power **6**, 28 (1990).
2. M. G. Millis, J. Propul. Power **13**, 577 (1997).
3. S. Batz and U. Peschel, Phys. Rev. Lett. **110**, 193901 (2013).
4. M. Wimmer, A. Regensburger, C. Bersch, M. A. Miri, S. Batz, G. Onishchukov, D. N. Christodoulides, and U. Peschel, Nat. Phys. **9**, 780 (2013).
5. J. Zhou, Y. Cheng, H. Zhang, G. Huang, and G. Hu, Theor. Appl. Mech. Lett. **5**, 196 (2015).
6. Y. Pei, Y. Hu, C. Lou, D. Song, L. Tang, J. Xu, and Z. Chen, Opt. Lett. **43**, 118 (2018).
7. N. N. Akhmediev and A. Ankiewicz, *Solitons: Nonlinear Pulses and Beams* (Chapman & Hall, 1997).
8. G. I. Stegeman and M. Segev, Science **286**, 1518 (1999).
9. J. S. Aitchison, A. M. Weiner, Y. Silberberg, D. E. Leaird, M. K. Oliver, J. L. Jackel, and P. W. E. Smith, Opt. Lett. **16**, 15 (1991).
10. M. Shalaby, F. Reynaud, and A. Barthelemy, Opt. Lett. **17**, 778 (1992).
11. J. Meier, G. I. Stegeman, Y. Silberberg, R. Morandotti, and J. S. Aitchison, Phys. Rev. Lett. **93**, 093903 (2004).
12. S. Liu, Y. Hu, P. Zhang, X. Gan, F. Xiao, C. Lou, D. Song, J. Zhao, J. Xu, and Z. Chen, Opt. Lett. **36**, 1167 (2011).
13. A. Smerzi, S. Fantoni, S. Giovanazzi, and S. R. Shenoy, Phys. Rev. Lett. **79**, 4950 (1997).
14. J. H. V. Nguyen, P. Dyke, D. Luo, B. A. Malomed, and R. G. Hulet, Nat. Phys. **10**, 918 (2014).
15. D. Mandelik, H. S. Eisenberg, Y. Silberberg, R. Morandotti, and J. S. Aitchison, Phys. Rev. Lett. **90**, 053902 (2003).
16. C. Kittel, *Introduction to Solid State Physics*, 5th ed. (Wiley, 1976).
17. F. Chen, M. Stepić, C. E. Rüter, D. Runde, D. Kip, V. Shandarov, O. Manela, and M. Segev, Opt. Express **13**, 4314 (2005).
18. Y. S. Kivshar, Opt. Lett. **18**, 1147 (1993).
19. Z. Chen, M. Segev, and D. N. Christodoulides, Rep. Prog. Phys. **75**, 086401 (2012).
20. J. W. Fleischer, M. Segev, N. K. Efremidis, and D. N. Christodoulides, Nature **422**, 147 (2003).
21. P. Zhang, S. Huang, Y. Hu, D. Hernandez, and Z. Chen, Opt. Lett. **35**, 3129 (2010).